Supplementary Information

Bifunctional aligned hexagonal/amorphous tungsten oxide core/shell nanorod arrays with enhanced electrochromic and pseudocapacitive performance

Xiangtao Huo,[a] Huanyu Zhang,[a] Weiguo Shen,[a] Xiwang Miao,[a] Mei Zhang[a] and Min Guo*[a]

[a] School of Metallurgical and Ecological Engineering, University of Science and Technology Beijing, Beijing 100083, P. R. China.

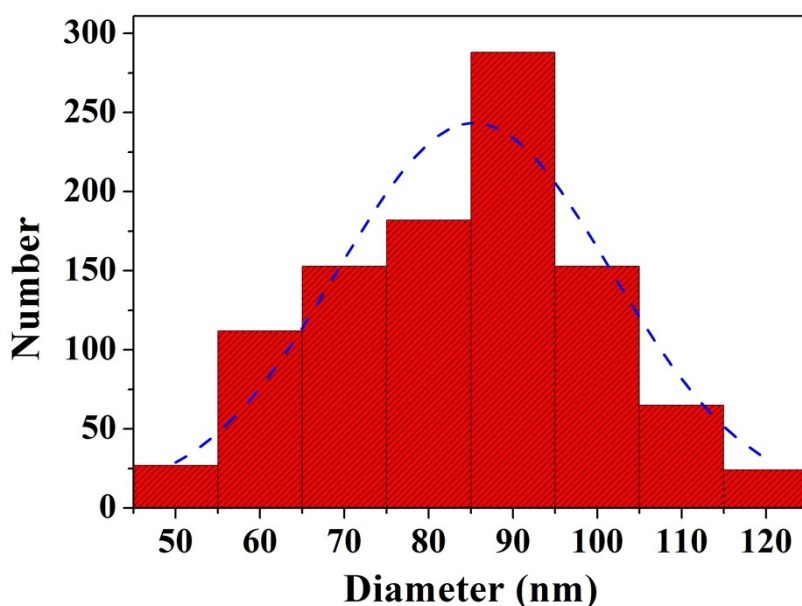E-mail: guomin@ustb.edu.cn; Fax: +86-10-6233-4926

Fig. S1 Statistics of diameter distribution of the h-WNRAs.

Fig. S1 illustrates the diameter distribution of the h-WNRAs. It can be seen that the average diameter of nanorods obtained by hydrothermal growth is about 85±15 nm, and over 75% of the nanorods fall into the range from 70 to 100 nm, which suggests that well-aligned WO_3 nanorods with uniform diameter can be fabricated.
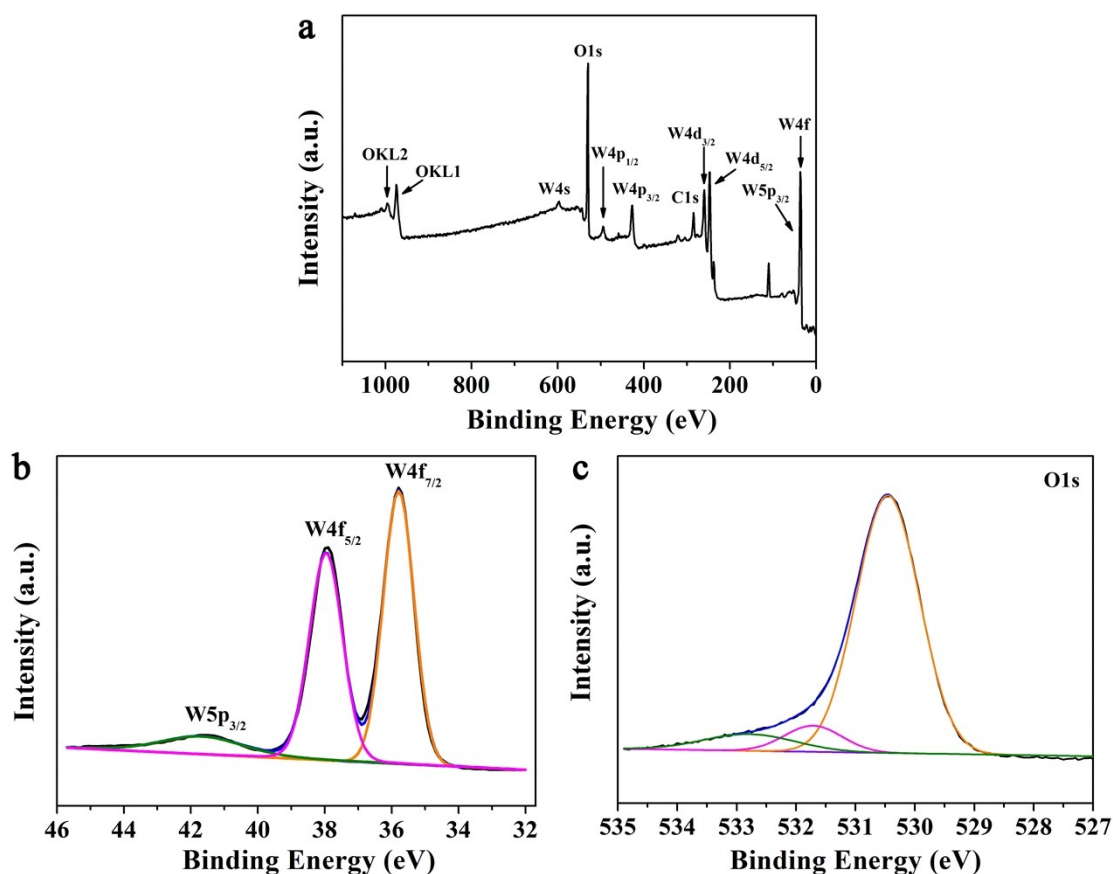
Fig. S2 XPS spectra for the WT 250-0.15: (a) full spectrum, (b) W4f and W5p, (c) O1s.

Fig. S2 illustrates the XPS spectra of WT 250-0.15, from the full spectrum (Fig. S2a), we can see that the main elements in nanorod arrays are W and O, which is consistent with the XRD results (Fig. 3 in the main article). Besides, according to the W4f and W5p core level spectrum in Fig. S2b, three peaks are in good separation located at 41.5 eV, 37.9 eV and 35.8 eV, corresponding to W $5p_{3/2}$, W $4f_{5/2}$ and W $4f_{7/2}$, respectively. These values match well with those reported in the previous literature [1,2], which can be reasoned that W in the nanorod arrays is at the highest oxidation state (W^{6+}). This demonstrates that the pure phase WO_3 grow on the FTO glass, which is consistent with the XRD results (Fig. 3 in the main article). Moreover, from the O1s core level spectrum (Fig. S2c), three peaks located at 530.5, 531.7 and 532.9 eV represent oxygen species in different ways, respectively. These values coincide with those of WO_3 reported previously.[3,4] The component located at 530.5 eV was assigned to oxygen atom (O^{2-})

that formed a strong bond in the manner W=O. The second peak at 531.7 eV might belong to a small mount hydroxyl group (OH^-) on the WO_3 surface. The third peak located at 532.9 eV may be the oxygen from the atmospheric water molecule that absorbed on the WO_3 surface. [3,4]
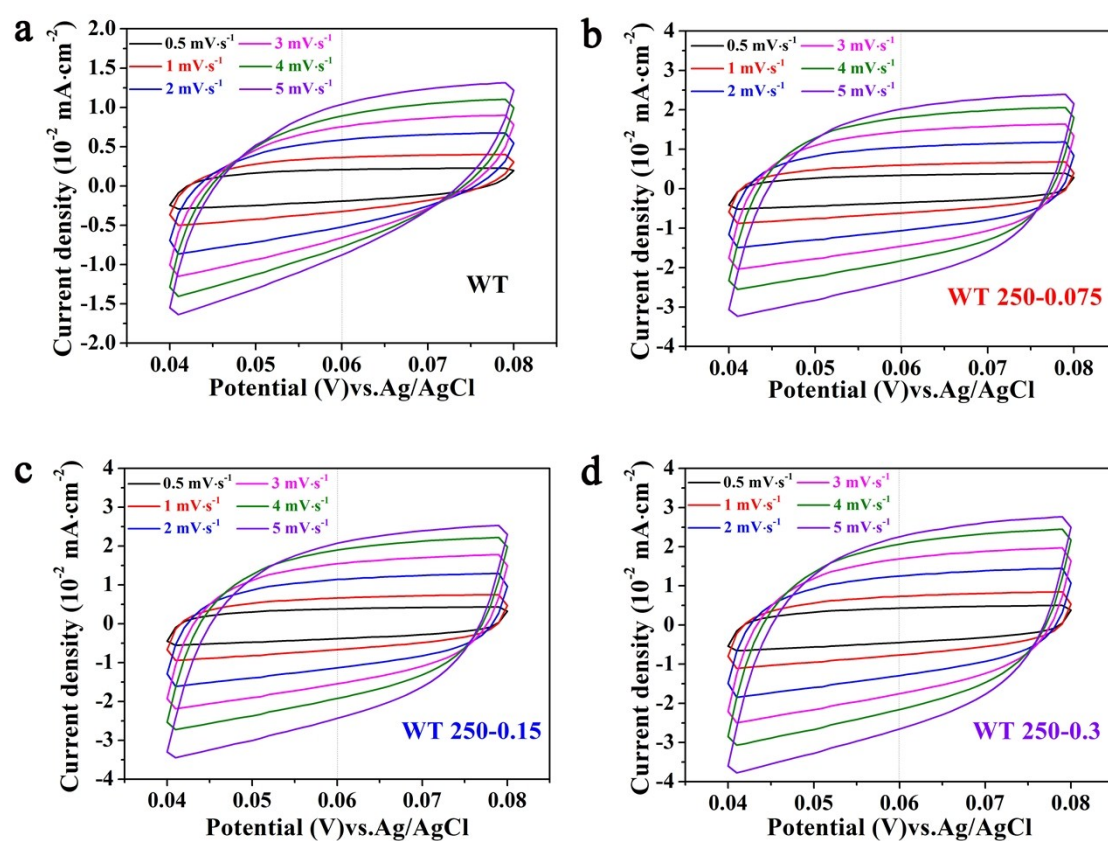

Fig. S3 The capacitive currents from double layer charging for various samples: (a) WT, (b) WT 250-0.075, (c) WT 250-0.15 and (d) WT 250-0.3.

The specific surface areas of the four samples were tested by cyclic voltammetry,[5, 6] that is to say, by measuring the pure double layer capacitances of the four samples within a tiny potential range in CV curves, the specific surface areas can be calculated according to the following formulas (1-2). The CV curves for measuring the pure double layer capacitances are as shown in Fig. S3. And results show that the specific surface areas (electrochemically active surface area (ECSA) of WNRAs per unit

geometric area (GA) of the FTO glass, $cm^2_{(ECSA)}/cm^2_{(GA)}$) of the four samples are calculated to be 41.2 $cm^2_{(ECSA)}/cm^2_{(GA)}$, 91.3 $cm^2_{(ECSA)}/cm^2_{(GA)}$, 94 $cm^2_{(ECSA)}/cm^2_{(GA)}$ and 102.7 $cm^2_{(ECSA)}/cm^2_{(GA)}$, respectively. It is obvious that the specific surface area of nanorods becomes larger by coating amorphous tungsten oxide. Detailed analysis are as follows:

The capacitive currents were measured in a tiny potential range where no Faraday process occurred, that is, there was no pseudocapacitive effect emerging. Only double layer capacitance was generated within the potential range, while its value only depends on the capacitive characteristics of the material itself and the size of its surface area. Therefore, the specific surface area of a specific material can be obtained by measuring its pure double layer capacitance.

The specific capacitance for a flat surface in aqueous solution is usually found to be about 20−60 $\mu F \cdot cm^{-2}$. In the following calculations of WT samples, we assume 40 $\mu F\ cm^{-2}$ as a moderate value. By testing the pure double layer capacitance (i.e., only nonfaradic process happened), we can convert it into specific area by the following formulas [5]:

$$A_{ECSA/GA} = \frac{C_{GA}}{40\ \mu F \cdot cm^{-2}\ per\ cm^2_{(ECSA)}} \tag{1}$$

where $A_{ECSA/GA}$ is the specific surface area (electrochemically active surface area (ECSA) of WNRAs per unit geometric area (GA) of the FTO glass, $cm^2_{(ECSA)}/cm^2_{(GA)}$), C_{GA} is the specific capacitance (capacitance of electrically active materials per unit geometric area of FTO glass, $F/cm^2_{(GA)}$), 40 $\mu F \cdot cm^{-2}$per $cm^2_{(ECSA)}$ stands for double layer capacitance per unit ECSA of WNRAs.

Herein, we measured the capacitive currents at a potential range in which no faradic process was observed, i.e., at 0.04-0.08 V versus Ag/AgCl. The CV curves (0.5-

5 mV·s^{-1}) of the four samples were measured by using a three-electrode system (FTO glass that coated with WNRAs as working electrode, Pt wire as counter electrode, Ag/AgCl as reference electrode). Meanwhile, 1 mol·L^{-1} H$_2$SO$_4$ was used as electrolyte.

The specific capacitance can be calculated by the following formula according to the literature [7]:

$$C_{GA}=\frac{1}{2v\Delta V}\int_{V_0}^{V_0+\Delta V}\frac{I}{A_{GA}}dV \qquad (2)$$

where C_{GA} represents the specific capacitance (capacitance of electrically active materials per unit geometric area of FTO glass, F/cm^2$_{(GA)}$); A_{GA} represents the total geometric area of FTO glass (cm^2$_{(GA)}$); v is the scan rate (mV/s); ΔV represents the potential range of test (V); V_0 is the initial potential (V); I represents the response current (A).

As shown in the Fig. S3, the approximately rectangular CV curves are obtained, which conform to the characteristics of double-layer capacitance. It can be concluded that only double-layer effect emerged in the samples within this potential range. The data obtained at the scan rate of 5 mV·s^{-1} is selected as the final result. Sample WT is taken as an example, the calculation process of specific surface area is as follows:

Firstly, the specific double layer capacitance (C_{GA}) can be calculated according to the formula 2, here $\frac{I}{A_{GA}}$ (i.e. current density), V_0 (initial potential=0.04 V), ΔV (potential range=0.04 V) and v (scan rate=0.005 V·s^{-1}) are as shown in the Fig. S3a. Bringing these values into the formula 2 $C_{GA}=\frac{1}{2\times0.005\times0.04}\int_{0.04}^{0.04+0.04}\frac{I}{A_{GA}}dV$, the specific double layer capacitance (C_{GA}) is calculated to be 1.648×10^{-3} F/cm^2$_{(GA)}$. Secondly, the specific surface area ($A_{ECSA/GA}$) could be calculated by the formula (1)

$$A_{\text{ECSA/GA}} = \frac{1.648 \times 10^{-3} \text{F/cm}^2_{\text{(GA)}}}{40 \, \mu\text{F cm}^{-2} \text{ per cm}^2_{\text{(ECSA)}}}$$, and the final value is 41.2 cm^2 $_{\text{(ECSA)}}$/cm^2 $_{\text{(GA)}}$. The

specific areas of other three samples are calculated by the same method, and finally the

specific surface areas of the four samples are calculated to be about 41.2 cm^2 $_{\text{(ECSA)}}$/cm^2

$_{\text{(GA)}}$, 91.3 cm^2 $_{\text{(ECSA)}}$/cm^2 $_{\text{(GA)}}$, 94 cm^2 $_{\text{(ECSA)}}$/cm^2 $_{\text{(GA)}}$ and 102.7 cm^2 $_{\text{(ECSA)}}$/cm^2 $_{\text{(GA)}}$,

respectively. It is obvious that the specific surface areas of the nanorod arrays become

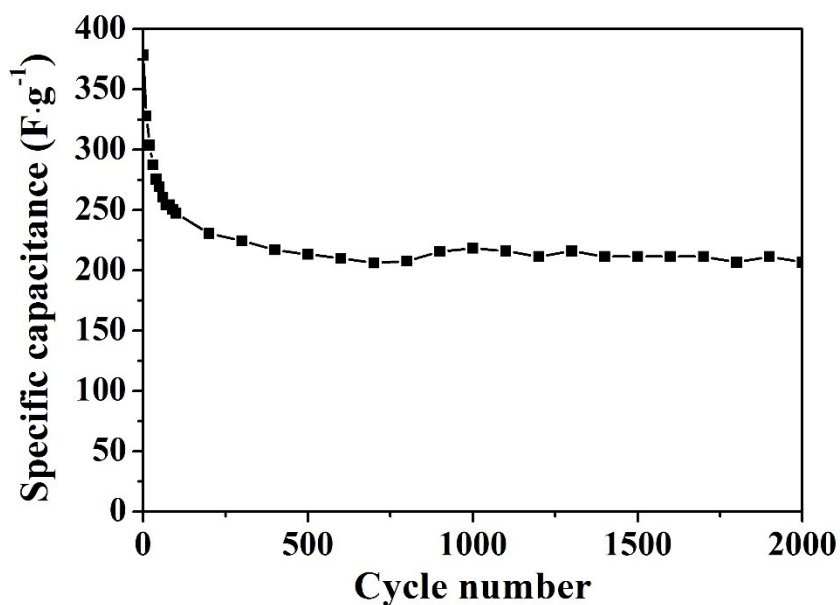larger by coating amorphous tungsten oxide films.

Fig. S4. Cycle performance of the sample WT 250-0.15 measured at 10 A·g^{-1} for 2000

cycles.

The results of constant current charge-discharge cycle test (Fig. S4) is similar to

that obtained by CV method in the main article (Fig. 7a). Both of them have an

activation process in the initial cycle stage, and then remain basically stable. Compared

with the initial value, the specific capacitance still retains 57.8% even after 2000 cycles.

Notes and references

1 D. Zhou, D. Xie, F. Shi, D.H. Wang, X. Ge, X.H. Xia, X.L. Wang, C.D. Gu and J.P. Tu, J. Colloid Interf. Sci., 2015, **460**, 200-208.

2 Y. Shimizu, A.C. Bose, D. Mariotti, T. Sasaki, K. Kirihara, T. Suzuki, K. Terashima and N. Koshizaki, Jpn. J. Appl. Phys. 2006, **45**, 8228-8234.

3 W.K. Man, H. Lu, L.C. Ju, F. Zheng, M. Zhang and M. Guo, Rsc Adv., 2015, **5**, 106182-106190.

4 V. V. Kondalkar, S. S. Mali, R. R. Kharade, R. M. Mane, P. S. Patil, C. K. Hong, J. H. Kim, S. Choudhury and P. N. Bhosale, RSC Adv., 2015, **5**, 26923–26931.

5 C.Y. Tang, W. Wang, A.K. Sun, C.K. Qi, D.Z. Zhang, Z.Z. W and D.Z. Wang, ACS Catal., 2015, **5**, 6956-6963.

6 X.D. Wen, L. Bai, M. Li, and J.Q. Guan, ACS Sustainable Chem. Eng., 2019, **7**, 9249−9256.

7 L. Wang, Y. L. Zheng, Q. Y. Zhang, L. Zuo, S. L. Chen, S. H. Chen, H. Q. Hou and Y. H. Song, RSC Adv., 2014, **4**, 51072-51079.